Inorganic Chemistry

Article

pubs.acs.org/IC

Diimine Triscarbonyl Re(I) of Isomeric Pyridyl-fulvene Ligands: an Electrochemical, Spectroscopic, and Computational Investigation

Daniel Chartrand, Carlos A. Castro Ruiz, and Garry S. Hanan*

Department of Chemistry, Université de Montréal, Montréal, Québec H3T 1J4, Canada

Supporting Information

ABSTRACT: The synthesis and characterization of a novel family of positively charged *fac*-[Re(bpy)(CO)$_3$(**L**)]PF$_6$ (bpy = 2,2′-bipyridine) complexes are reported, where **L** is a pyridine functionalized in *para* or *meta* position with a fulvene moiety, namely, 4-fluoren-9-ylidenemethyl-pyridine (***p*Fpy**) and 3-fluoren-9-ylidenemethyl-pyridine (***m*Fpy**). The complexes were prepared in high yield (86%) by direct addition at room temperature of the corresponding pyridine to the tetrahydrofuran (THF) adduct *fac*-[Re(bpy)(CO)$_3$(THF)][PF$_6$] precursor. Both ligand and complex structures were fully characterized by a variety of techniques including X-ray crystallography. The complexes did not exhibit the expected triplet mixed metal−ligand-to-ligand charge transfer (MLLCT) emission, because of its deactivation by the non-emissive triplet excited state of fulvene. The absorption profile shows that the MLLCT is overshadowed by the fulvene centered $\pi-\pi^*$ transition of higher molar absorptivity as shown by time dependent density functional theory (TD-DFT) calculations. The position of the fulvene on the pyridyl ring has a large effect on this transition, the *para* position displaying a much higher absorption coefficient (21.3×10^3 M^{-1} cm^{-1}) at lower energy (364 nm) than the meta position (331 nm, 16.0×10^3 M^{-1} cm^{-1})

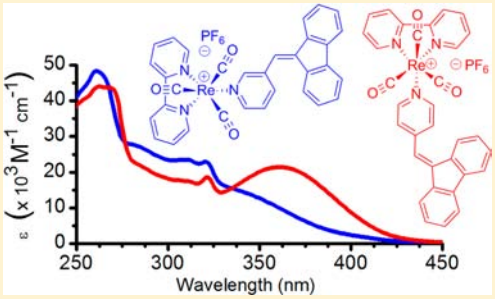

INTRODUCTION

Rhenium triscarbonyl diimine chromophores have been studied extensively for the past 30 years; their unique characteristics (e.g., high stability, high energy excited states, capacity for reductive and oxidative electron transfer) make them ideal for photosensitizers.[1] They are found as photoactive components in various roles: chromophores supplying electrons to catalysts (e.g., hydrogen evolution);[2] photocatalysts reducing carbon dioxide to carbon monoxide;[3] photosensitizers permitting visible light photoisomerization;[4] and as chromophoric building-blocks for supramolecular assemblies.[5] One common variant involves a 2,2′-bipyridine (bpy) ligand and a secondary neutral ligand L in complexes of the type [Re(bpy)(CO)$_3$L]$^+$, with pyridine being the motif of choice for further functionalization of the rhenium chromophore through ligand L. To expand the utility of the rhenium-bpy unit, a *meta* and *para* fulvene functionalized pyridine was used as ligand L in this study, and the chemical and photophysical properties of its rhenium complexes were determined.

The properties of the fulvene ligands are similar to those of stilbene molecules in that they can undergo isomerization through their triplet excited state,[6] albeit the irradiation energy necessary for this isomerization is often found only in the UV region unless highly conjugated molecules are used. In addition, the quantum yield of isomerization is usually relatively low because of the triplet state of the molecule competing with the permitted fluorescence decay of the singlet excited-state. As such, grafting a rhenium onto the fulvene core may enhance both the absorption, by causing its red-shift with a concomitant increase in the coverage of a broader spectrum of light, and the efficiency, by quenching the fluorescence to a longer-lived, higher-energy triplet state centered on the rhenium bipyridine that will act as a reservoir for the triplet state centered on the fulvene. This process is well described for Ru(II) diimine complexes containing fused polycyclic moieties.[7]

Although energy transfer has been investigated using rhenium complexes displaying intramolecular charge transfer more than 25 years ago,[8] recent research has examined the addition of photoisomerizable ligands, containing stilbene analogues and other moieties, that once coordinated quench the luminescence of the rhenium in favor of their isomerization.[4a−i] Closer to our design is the 4-styrylpyridine motif, which upon coordination to rhenium was shown to undergo photoisomerization with lower energy light and at higher efficiency by spectroscopic and high level computational studies.[4k−m] In our case, no isomerization is observable because of the symmetry of the ligand, but energy transfer can still be observed because of the absence of emission of the rhenium complex, suggesting that the non-radiative decay of the excited state passes by the triplet state of the fulvene. Another interesting aspect of this study is the delocalization of the fulvene orbitals onto the rhenium core, which is seen in only one of the pyridyl isomers.

EXPERIMENTAL SECTION

General Considerations. All of the organic reagents were obtained from Sigma Aldrich, rhenium carbonyl from Pressure Chemical Co. and solvents from Fischer and Anachemia and were used as received

Received: July 17, 2012
Published: November 15, 2012

   dx.doi.org/10.1021/ic301559s | *Inorg. Chem.* 2012, 51, 12738−12747

without any further purification. IR spectra were recorded on solid samples using a diamond ATR Perkin-Elmer Spectrum 100 FT-IR. Nuclear magnetic resonance spectra were recorded using Bruker spectrometers (300 and 400 MHz) at room temperature, with ^{1}H and ^{13}C chemical shifts referenced to residual solvent resonances. Elemental analyses were performed on the desolvated bulk samples by the university departmental service. Room temperature Photophysical measurements were done in air-equilibrated and degassed freshly distilled dichloromethane (DCM), using a quartz cell. Low-temperature emission were recorded in degassed 1 MeOH: 4 EtOH (v:v) and 1 toluene: 1 DCM (v:v) glasses at 77 K in a borosilicate tube. Absorption and emission spectra were recorded using a Cary 500i UV−vis−NIR spectrophotometer and a Cary Eclipse 300 fluorimeter, respectively. Oscillator strengths and peak maxima are obtained from integrated fitted Gaussian curves of the molar absorptivity spectrum in function of wavenumber, following the following equation: $f = 1.44 \times 10^{-9} \int \varepsilon(\nu)\, d\nu$. The emission spectra used the maximum of absorption of the lowest energy band of the studied molecules as excitation wavelength. Electrochemical measurements were carried out in argon-purged DCM at room temperature with a BAS CV50W multipurpose equipment interfaced to a PC. The working electrode was a Pt electrode, the counter electrode was a Pt wire, and the pseudoreference electrode was a silver wire. The reference was set using an internal 1.0 mM ferrocene/ferrocinium sample with its redox couple adjusted to 460 mV vs SCE in dichloromethane.[9] The concentration of the compounds was around one mM. Tetrabutylammonium hexafluorophosphate (TBAP) was used as supporting electrolyte, and its concentration was 0.10 M. Cyclic voltammograms (CVs) were obtained at scan rates of 50 and 100 mV/s. For reversible processes, half-wave potentials (vs SCE) were measured with square wave voltammetry (SWV) experiments performed with a step rate of 4 mV, a square wave amplitude of 25 mV, and a frequency of 15 Hz. For irreversible oxidation processes, the cathodic peak was used as *E*, and the anodic peak was used for irreversible reduction processes. The criteria for reversibility were the separation of 60 mV between cathodic and anodic peaks, the close to unity ratio of the intensities of the cathodic and anodic currents, and the constancy of the peak potential on changing scan rate. Experimental uncertainties are as follows: absorption maxima, ± 2 nm; molar absorption coefficient, 10%; emission maxima, ± 5 nm; redox potentials, ± 10 mV.

Synthetic Methods. The rhenium complexes $Re(CO)_5Br$,[10] *fac*-$[Re(bpy)(CO)_3Br]$,[11] *fac*-$[Re(bpy)(CO)_3(MeCN)][PF_6]$,[12] *fac*-$[Re(bpy)(CO)_3(pyridine)][PF_6]$ (**3**), and *fac*-$[Re(bpy)(CO)_3(THF)][PF_6]$[13] were prepared following the literature procedures. The ligands ***m*Fpy** and ***p*Fpy** were prepared by a modified literature method.[14] They have been synthesized by a similar route before, but with only basic characterization.[15] Herein, their free base versions are fully characterized. See Supporting Information, Chart S1 for the labeling of the proton peaks in NMR. Note that the hydrochloride salts were characterized more recently by proton NMR as well.[16]

3-((9*H*-fluoren-9-ylidene)methyl)pyridine (*m*Fpy). Fluorene (4.023 g, 24.2 mmol) and KOH (2.028 g, 36.1 mmol) were taken in ethylene glycol dimethyl ether (35 mL) in a round bottomed flask and stirred at reflux for 10 min. 3-Pyridinecarboxaldehyde (3.89 g, 36.3 mmol) was added dropwise, and the stirring was continued at the same temperature for 4 h, during which the initial red mixture turned dark green. After the mixture was cooled to room temperature, water (200 mL) was added, and the mixture stirred at ambient temperature for 45 min, resulting in a yellow-orange suspension. The suspension was isolated by filtration, and the resulting yellow precipitate was washed with hexane (4 × 40 mL) and purified by column chromatography (Al_2O_3, DCM/AcOEt (v:v) (1:1)) to afford a pale yellow pure compound. Yield: 70%.^{1}H NMR ($CDCl_3$ 300 MHz) δ ppm 8.85 (s, 1He), 8.65 (d, J = 4 Hz, 1Hf), 7.89 (d, J = 8 Hz, 1Hh), 7.78 (d, J = 7 Hz, 1Hj), 7.71 (d, J = 7 Hz, 2Hmm′), 7.57 (s, 1Hi), 7.45−7.37 (m, 3Hgj′k), 7.34 (ddt, J = 7, 3, 1 Hz, 2Hll′), 7.06 (dt, J = 8, 1 Hz, 1Hk′). $^{13}C\{^{1}H\}$ NMR (75 MHz, $CDCl_3$) δ ppm 150.2, 149.0, 141.5, 139.4, 138.9, 138.5, 136.5, 136.1, 133.9, 129.1, 128.7, 127.2, 126.9, 124.2, 123.3, 122.6, 120.4, 119.9, 119.7. HRMS (ESI, MeCN) (m/z): $[M+H]^+$ ($C_{19}H_{14}N$) calcd 256.11207; found 256.11255. Anal. Calcd for $C_{19}H_{13}N$: C, 89.38; H, 5.13; N, 5.49. Found: C, 88.85; H, 5.11; N, 5.28.

4-((9*H*-fluoren-9-ylidene)methyl)pyridine (*p*Fpy). Synthesized as the previous example, purification by crystallization from ethyl acetate/hexane (1:2 v:v) instead of column chromatography. Afforded pale yellow crystalline product. Yield: 38−50%. ^{1}H NMR (300 MHz, $CDCl_3$) δ ppm 8.71 (d, J = 6 Hz, 2He), 7.76 (d, J = 8 Hz, 1Hh), 7.70 (d, J = 8 Hz, 2Hmm′), 7.50 (s, 1Hi), 7.48 (d, J = 5 Hz, 2Hf), 7.44 (d, J = 8 Hz, 1Hj′), 7.41 (dt, J = 7, 1 Hz, 1Hk), 7.34 (dt, J = 7, 1 Hz, 2Hll′), 7.06 (dt, J = 7, 1 Hz, 1Hk′). $^{13}C\{^{1}H\}$ NMR (75 MHz, $CDCl_3$) δ ppm 150.2, 141.6, 140.3, 139.5, 138.8, 138.7, 135.9, 129.3, 129.0, 127.2, 126.9, 124.5, 123.8, 123.2, 120.5, 120.0, 119.7. HRMS (ESI, MeCN) (m/z): $[M+H]^+$ ($C_{19}H_{14}N$) calcd 256.11207; found 256.11240. Anal. Calcd for $C_{19}H_{13}N$: C, 89.38; H, 5.13; N, 5.49. Found: C, 89.35; H, 5.17; N, 5.50.

3-((9*H*-fluoren-9-ylidene)methyl)pyridine-2,2-bipyridine-tricarbonyl-rhenium(I) Hexafluorophosphate [Re(bpy)-(CO)$_3$(*m*Fpy)][PF$_6$]. (**1**) Under an inert atmosphere, *fac*-$[Re(bpy)(CO)_3(THF)][PF_6]$ (79.3 mg, 123 μmol) and ***m*Fpy** (32.2 mg, 126 μmol) were mixed in THF (5 mL) and left to stir for 16 h at room temperature. The product was then precipitated by addition of hexane (50 mL), resulting in a yellow solid. The product was purified by dissolution in a minimum of dichloromethane (2 mL) with a few drops of toluene and followed by slow evaporation of DCM in a closed, toluene-containing jar, affording a pale yellow solid. Yield: 87.0 mg (105 μmol) (86%). ^{1}H NMR (400 MHz, $(CD_3)_2CO$) δ ppm 9.48 (ddd, J = 5, 2, 1 Hz, 2Ha), 8.76 (d, J = 8 Hz, 2Hd), 8.72 (dd, J = 2, 1 Hz, 1He), 8.66 (d, J = 5 Hz, 1Hf), 8.41 (dt, J = 8, 2 Hz, 2Hb), 8.22 (d, J = 8 Hz, 1Hh), 7.90 (ddd, J = 8, 5, 1 Hz, 2Hc), 7.83 (d, J = 8 Hz, 3Hjmm′), 7.66 (dd, J = 8, 5 Hz, 1Hg), 7.58 (s, 1Hi), 7.45 (dt, J = 8, 1 Hz, 1Hk), 7.37 (ddd, J = 13, 8, 1 Hz, 2Hll′), 6.97 (dt, J = 8, 1 Hz, 1Hk′), 6.77 (d, J = 8 Hz, 1Hj′). $^{13}C\{^{1}H\}$ NMR (75 MHz, $(CD_3)_2CO$) δ ppm 196.3, 156.8, 154.9, 152.8, 152.2, 142.4, 142.4, 141.2, 140.43, 140.35, 139.4, 137.3, 136.3, 130.43, 130.26, 129.96, 128.36, 128.23, 127.8, 125.8, 124.4, 121.84, 121.28, 121.19, 120.7. HRMS (ESI, MeCN) (m/z): $[M]^+$ ($C_{43}H_{21}N_3O_3{}^{187}Re$) calcd 682.11349; found 682.11275. IR (ATR, cm^{-1}) ν_{CO}: 2031s, 1944s, 1911s; ν_{PF} 837s. Anal. Calcd for $C_{32}H_{21}F_6N_3O_3PRe$ + 0.5 toluene: C, 48.85; H, 2.89; N, 4.81. Found: C, 48.53; H, 2.76; N, 4.81.

4-((9*H*-fluoren-9-ylidene)methyl)pyridine-2,2-bipyridine-tricarbonyl-rhenium(I)hexafluorophosphate [Re(bpy)-(CO)$_3$(*p*Fpy)][PF$_6$]. (**2**) Complex **2** was synthesized in the same manner as the previous example. The product was purified by dissolution in a minimum of chloroform (2 mL) with a few drops of ethyl acetate and crystallized by slow diffusion of ethyl acetate in a closed jar. Yield: 90.0 mg (108 μmol) (86%). ^{1}H NMR (400 MHz, $(CD_3)_2CO$) δ ppm 9.54 (ddd, J = 6, 2, 1 Hz, 2Ha), 8.79 (d, J = 8 Hz, 2Hd), 8.64 (dd, J = 5, 2 Hz, 2He), 8.51 (dt, J = 8, 2 Hz, 2Hc), 8.04 (ddd, J = 8, 3, 1 Hz, 2Hb), 7.83−7.79 (m, 3Hjmm′), 7.68 (dd, J = 7, 1 Hz, 2Hf), 7.60 (s, 1Hi), 7.42 (dt, J = 8, 1 Hz, 1Hk), 7.38 (dt, J = 8, 1 Hz, 1Hl′), 7.33 (dt, J = 8, 1.0 Hz, 1Hl), 7.25 (d, J = 8 Hz, 1Hj′), 7.01 (dt, J = 8, 1 Hz, 1Hk′). $^{13}C\{^{1}H\}$ NMR (75 MHz, $(CD_3)_2CO$) δ ppm 196.5, 156.8, 155.0, 153.1, 149.8, 142.88, 142.37, 141.2, 140.4, 139.5, 135.9, 130.97, 130.56, 130.07, 128.5, 127.89, 127.78, 125.76, 125.05, 122.62, 122.01, 121.2, 120.8. HRMS (ESI, MeCN) (m/z): $[M]^+$ ($C_{43}H_{21}N_3O_3{}^{187}Re$) calcd 682.11349; found 682.11374. IR (ATR, cm^{-1}) ν_{CO}: 2028s, 1925s, 1903s; ν_{PF} 832s. Anal. Calcd for $C_{32}H_{21}F_6N_3O_3PRe$: C, 46.49; H, 2.56; N, 5.08. Found: C, 46.56; H, 2.50; N, 4.99.

Computational Methods. All calculations were performed with the Gaussian 03 software.[17] All models used crystallographic structure data as starting point for ground-state geometry optimization (singlet and triplet). The geometry optimization was carried out with the density functional theory (DFT) method using the B3LYP functional in the gas phase.[18] The 6-31G** basis set was used for C, H, N, and O while the relativistic LANL2DZ with effective core potentials and one additional f-type polarization function was implemented for the Re atom (α_f = 0.890).[19] Energy levels and frequencies for both singlet and triplet optimized geometries were calculated using single-point energy calculation with a polarized continuum model (PCM) using dichloromethane as solvent.[20] The absorption spectra properties in DCM were calculated by the time-dependent DFT (TD-DFT) approach

Table 1. Crystal Data and Structure Refinement Information for *m*Fpy, *p*Fpy, 1, and 2

	*m*Fpy	*p*Fpy	1	2
formula	$C_{19}H_{13}N$	$C_{19}H_{13}N$	$[C_{32}H_{21}N_3O_3Re][F_6P]\cdot 0.5(C_4H_8O_2)$	$[C_{32}H_{21}N_3O_3Re][F_6P]\cdot CH_2Cl_2$
cryst. syst.	triclinic	monoclinic	orthorhombic	triclinic
space grp	$P\bar{1}$	$P2_1/c$	$Pca21$	$P\bar{1}$
a (Å)	6.2909(4)	9.2782(4)	29.1631(5)	8.1758(3)
b (Å)	11.8465(7)	21.8542(9)	12.2319(2)	14.2872(5)
c (Å)	18.5314(11)	6.9306(3)	18.7356(44)	14.8093(5)
α (deg)	90.475(3)	90	90	90.429(1)
β (deg)	96.308(3)	104.675(2)	90	90.852(2)
γ (deg)	105.025(3)	90	90	102.281(2)
V (Å^3)	1324.79(14)	1359.46(10)	6683.4(2)	1689.99(10)
Z	4	4	4	2
R1; wR2	0.0472;	0.0422;	0.0263;	0.0313;
($I > 2\sigma(I)$)	0.1151	0.1111	0.0730	0.0832
R1; wR2	0.0685;	0.0466;	0.0258;	0.0313;
(all data)	0.1227	0.1142	0.0735	0.0833
GoF (F^2)	0.985	1.035	1.065	1.089
Flack par.	n.a.	n.a.	−0.002(6)	n.a.

associated with the polarized continuum model (PCM).[20] GaussSum 2.2 was employed to draw absorption spectra (simulated with Gaussian distribution with a full-width at half-maximum (fwhm) set to 3000 cm^{-1}) and extract the atomic orbital population information from calculated data.[21]

Crystal Structure Determination. X-ray crystallographic data were collected from a single crystal sample, which was mounted on a loop fiber. For both ligands, data were collected with a Bruker Platform diffractometer, equipped with a Bruker SMART 4K Charged-Coupled Device (CCD) Area Detector and a Nonius FR591 rotating anode Cu Kα X-ray radiation source equipped with a Montel 200 optics at 200 (2) K. For the two complexes, data were collected with a Bruker Microstar diffractometer equipped with a Platinum 135 CCD Detector at 150 (2) K. The data was integrated with APEX2 software and corrected for absorption using the SADABS package.[22] Following analytical absorption corrections and solution by direct methods, the structures were refined against F^2 with full-matrix least-squares using the program SHELXL-97.[23] All H-atoms were added at calculated positions and refined by use of riding models with isotropic displacement parameters based on those of the parent atoms. Anisotropic displacement parameters were employed throughout for the non-hydrogen atoms. Images were generated using Ortep III and Pov-Ray.[24] X-ray quality crystals were obtained from slow evaporation of a chloroform solution for the ligands ***p*Fpy** and ***m*Fpy**. Crystals of **1** were obtained by slow diffusion of ethyl acetate into a chloroform solution of **1**. Complex **2** crystallized following the given purification procedure. Specific parameters of each measurement are located in Table 1. Note that ***p*Fpy** has been reported before but without any complete data set deposited in the Cambridge structural database.[15b]

RESULTS AND DISCUSSION

The ligands were synthesized by a condensation reaction between fluorene and pyridinecarboxaldehyde, following a slightly modified protocol for benzylidene-fluorene synthesis.[14] Established procedures for the synthesis of 9-pyridylidenefluorene, studied mainly for their medicinal properties, are less accessible synthetically.[15a,16] Our first attempts to coordinate the ligands to the rhenium ion, using the precursor [Re(bpy)(CO)$_3$(acetonitrile)][PF$_6$] and 10 equiv of the ligand, following an established methodology, produced only moderate yields.[12] [Re(bpy)(CO)$_3$(THF)][PF$_6$], first reported in 1985, was a better starting material as it is easily synthesized and is much more reactive, as the THF adduct exchanges neatly at room temperature with only 1 equiv of the pyridyl ligand (Chart 1).[13] Near quantitative yields were obtained, and no purification was needed prior to crystallization.

Chart 1. Synthesis of the Rhenium Chromophores with the Labeling of the Species

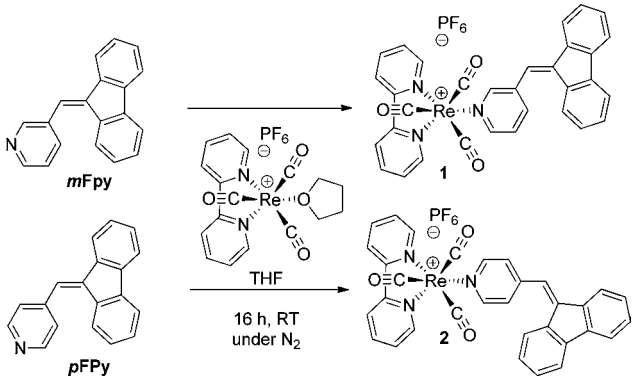

The IR spectra of both complexes are consistent with the facial configuration of the carbonyl ligands as indicated by three intense absorptions, which are observed in the 2031 to 1911 cm^{-1} region for **1** and the 2028 to 1903 region for **2**. These bands are similar to other rhenium complexes, for example, [Re(bpy)(CO)$_3$(pyridine)][CF$_3$SO$_3$] (**3**), that has bands at 2026, 1921, and 1907 cm^{-1}.[25] No bands around 1600 cm^{-1} could be clearly identified as being part of the fulvene vinyl group, as they are masked by the other C=C stretches of the bipyridine and pyridine.

The proton chemical shifts remain essentially the same for both complexes, the biggest change is the downfield shift of the fluorene proton nearest to the vinyl proton of complex **1** (j′ see Chart S1 for labeling in Supporting Information). The chemical shift passes from 7.45 ppm to 6.77 ppm for **1** vs 7.25 ppm for **2**. This extra shielding comes from the Re(bpy)(CO)$_3$ fragment as it is nearer in the *meta* version because of the free rotation of the pyridyl group along its single bond to the fulvene core. The pyridine protons *ortho* to the nitrogen ligand shift to similar amounts upon coordination to the metal center (8.66 and 8.72 ppm for **1** vs 8.64 ppm for **2**), as expected.

Both ligand and complexes were fully characterized by X-ray crystallography and have excellent structure quality, with disorder present for the complexes only on the PF$_6$ counterion or co-crystallized solvent. It is noteworthy that complex **1** and ***m*Fpy** crystallized as two independent molecules in the asymmetric unit

dx.doi.org/10.1021/ic301559s | Inorg. Chem. 2012, 51, 12738−12747

cell, which gives a good indication on the precision of the bond lengths and inherent variability of the spatial arrangement of the atoms. Full unit-cell views of all molecules are found in the Supporting Information, Figures S1 to S4.

The fulvene ligands are similar in structure, with the pyridyl ring being rotated out of the plane of the fluorene ring. The angle of rotation is more dependent on the packing itself, as there is a notable difference in the angle for the two crystallographically independent molecules of ***m*Fpy** (50.4° and 41.6°), while ***p*Fpy** has an angle is 60.8°. In the complexes these angles become 36.5° for complex **1** (both molecules have the same angle) and 45.9° for **2**.

The planarity of the fluorene is a good indication of its conjugation; it is measured by the angle of both planes formed by each fused phenyl ring. Both ligands and complexes show a similar planarity with no significant variations. The biggest angle change is seen for the two crystallographically independent molecules of **1** at 4.5° and 2.8°, giving an almost 2° shift as a normal fluctuation because of crystal packing. The ***m*Fpy** ligand has distortion angles of 4.6° and 5.1°, the ***p*Fpy** ligand is at 3.9° (also reported at 4.1°)[15b] while in **2** it is at 4.4°. There is clearly no effect on the distortion angle from the coordination of rhenium to the ligand and no appreciable differences between the *meta* and *para* ligands.

A look at the length of the double bond bridging the pyridyl and the fluorene shows an average distance of 1.35 ± 0.01 Å (for both ligand and **1**); in the case of **2**, it is shorter at 1.318(8) Å. This could imply a stronger double bond and can be rationalized looking at the reduced torsion angle present in the vinyl bond of **2** (5 ± 1° for **2** versus 10 ± 2° for **1**). The increased planarity of the vinyl bond in **1** brings the twisted pyridine ring closer to the fulvene plane.

The rhenium centers have standard coordination geometry. The CO bonds are not significantly different, as can be shown in the case of the two distinct molecules present for **1**, where up to 0.02 Å variations can be observed for otherwise identical carbonyl environments. As shown in Figure 1, there is an observable coplanarity of the rhenium core (the plane formed by N3, N2, C32, and C30) and the fluorene moiety in the case of complex **2**; the rhenium atoms are lying only 0.17 Å above the plane, and there is an angle of only 2° between the fluorene and the rhenium cores. In the case of **1** the geometry of the rhenium core is completely twisted off the fluorene plane. The coplanarity of the rhenium core with the fulvene in **2** will be shown to have a role in its electronic properties despite the 45° rotation of the pyridine ring.

Electrochemistry. The electrochemistry reveals the energy of the highest occupied molecular orbital (HOMO) and lowest unoccupied molecular orbital (LUMO) and can give important information about the energy levels involved in electronic transitions.

On the oxidation side, a rhenium pyridyl complex should have a partially reversible oxidation around 1.85 V vs SCE in dichloromethane.[26] Also we can have oxidation of the fulvene ligand, measured as an irreversible oxidation at 1.72 V vs SCE (in CH_2Cl_2), very close to the reported 1.67 V for the closest analogue, 9-benzylidenefluorene.[27] As reported in Table 2 and Supporting Information, Figure S5, both complexes **1** and **2** have an oxidation at 1.84 V vs SCE in CH_2Cl_2. It is difficult to assign this redox couple as either the expected Re(I)/Re(II) or as Fpy/$Fpy^{+\cdot}$ or both. A square-wave voltammetry suggests an electron count of at least two, implying both redox couples are occurring in the same region (Supporting Information, Figure S6).

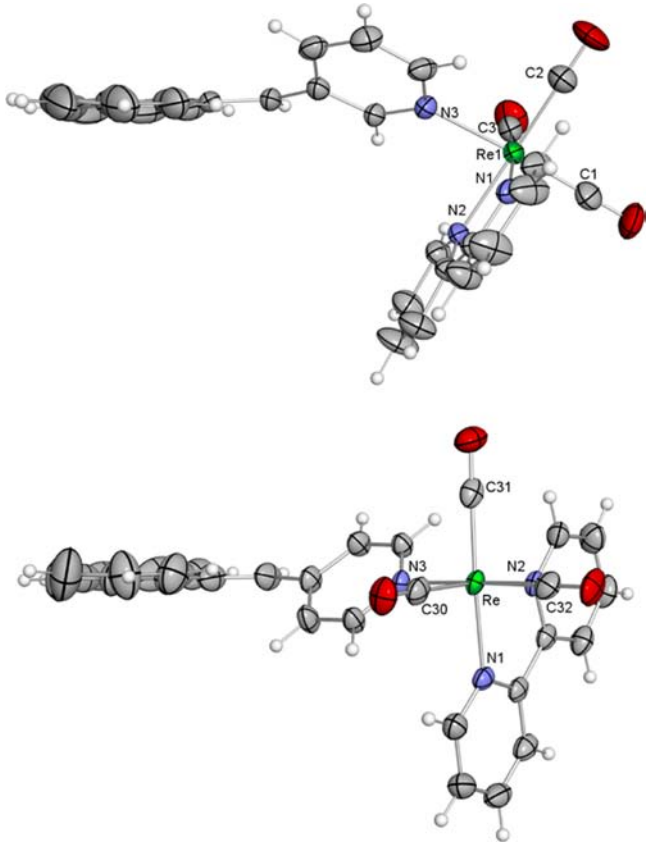

Figure 1. ORTEP view of the X-ray crystal structures of **1** (top) and **2** (bottom) along the fulvene plane (50% probability displacement ellipsoids; anion, solvent, and other chemically equivalent molecule removed).

On the reduction side, two redox couples are reported to be centered on the bipyridine ligand of complex **3**.[26] The first is reversible at −1.2 V and the other is irreversible and reported at −1.7 V. From the electrochemistry of the free **Fpy** ligand, we expect a semi-reversible reduction centered as low as −1.55 V, but because of the electron withdrawing effect of the rhenium, this reduction could occur at less negative potential.

Complexes **1** and **2** have four reduction processes. In the case of **1**, only three reduction waves are seen; in this case the first reduction wave is broad, at −1.10 V (160 mV width), and suggests a ratio of two-to-one electrons as compared to the second reduction wave observed at −1.45 V (Supporting Information, Figure S6), suggesting that two unresolved reductions occur next to each other. This suggestion is sustained by the CV of **2**, showing two distinct and reversible peaks located at −1.08 and −1.23 V. The first reduction is without a doubt the bpy/$bpy^{\bullet-}$ redox couple, the second one has no choice to be centered on the fulvene ligand, since in **3** the second reduction of the bpy is at a much more negative potential (−1.7 V). Since a third wave is seen for both complexes around −1.45 V, two redox couples are centered on the fulvene ligand even if in the case of the free molecule only one was observable. The first one, in the case **1**, occurs at slightly more negative potential than the bpy reduction and overlaps with it. While for **2**, there is a clean separation between the peaks, this can be partly due to the higher delocalization of the fulvene, enabling it to interact more with the singly reduced bpy and push its own reduction to a more negative potential; this delocalization will be further discussed with the spectral data. The second reduction of the fulvene is at

dx.doi.org/10.1021/ic301559s | *Inorg. Chem.* 2012, 51, 12738−12747

Table 2. Electrochemical Data of the Complexes in CH_2Cl_2, Bu_4NPF_6 (0.1 M) Electrolyte

	$E_{1/2}^{ox}$ (ΔE (mV))	$E_{1/2}^{red}$ (V) (ΔE (mV))			
	Re^{II}/Re^{I} ($Fluo^{+\cdot}/Fluo$)	$bpy/bpy^{-\cdot}$	$Fluo/Fluo^{-\cdot}$	$Fluo^{-\cdot}/Fluo^{-2}$	$bpy^{-\cdot}/bpy^{-2}$
1	1.84 (250)	−1.11 (160)[a]		−1.45 (230)	−1.71 (irr)
2	1.84 (120)	−1.08 (66)	−1.23 (60)	−1.434 (230)	−1.74 (irr)
3[b]	1.85 (irr)	−1.2 (60)			−1.7 (irr)
Fpy[c]	1.72 (irr)		−1.55 (260)		

[a]Unresolved two one-electron reductions. [b]From literature, triflate salt with Bu_4NPF_6(0.2 M) electrolyte.[26] [c]***m*Fpy** and ***p*Fpy** gave the same result.

Table 3. Measured and Calculated Electronic Absorption Properties of the Re Complexes and Ligand in DCM

	λ_{max} (nm); (ε (cm^{-1} M^{-1})); [f (a.u.)]						
	lowest energy transition			bpy transition		fluorene transition	
		calc.			calc.		calc.
	expt.	Fp→Fpy	Re→bpy	expt.	bpy→LUMO	expt.	fluorene→LUMO
***m*Fpy**	330 (15000) [0.27]	347 [0.65]				260 (39000) [0.22]	259 [0.48]
***p*Fpy**	327 (13600) [0.25]	347 [0.60]				260 (41100) [0.25]	261 [0.61]
1	331 (16000) [0.45]	367 [0.49]	360 [0.02] 373 [0.13]	321 (22800) [0.009]	299 [0.16]	261 (48300) [0.29]	260 ± 1 [0.53][b]
2	364 (21300) [0.43]	397 [0.79]	358 [0.04] 365 [0.03]	321 (18500) [0.010]	300 ± 4 [0.16][a]	263 (44000) [0.35]	262 ± 1 [0.44][b]
3	359 (4800) [0.13]		361 [0.01] 375 [0.10]	321 (13500) [0.015]	300 [0.14]		

[a]Total oscillator strength of all stated transitions in a ±4 nm range. [b]In a ± 1 nm range.

more or less the same potential of **1** at −1.45 V. Finally, the second irreversible bpy reduction is seen in the expected range for both complexes.

The electrochemistry does not allow clear identification of the individual processes occurring on the oxidation side, but it is clear on the reduction side that the bpy is the first to reduce, then the **Fpy** ligand follows. In term of energy gap, all of the complexes have a HOMO LUMO gap around 2.94 (±0.02) V, suggesting again very little effect of the **Fpy** toward the rhenium core and that the oxidation potential of **Fpy** is very closely matched to that of its rhenium complex.

Photophysical Investigation and Comparison with Theoretical Models. The absorption spectra of the ligands as well as of the complexes were measured in dichloromethane solutions and are compared to the TD-DFT calculations, with a solvent dielectric potential to simulate solvation. It is noteworthy that these calculations only take into account the singlet-state transitions. In the case of rhenium complexes, there can be some absorption from triplet-state transitions due to the spin−orbit coupling induced by heavy atoms, but these effects are not modeled using Gaussian03.[28] Although the calculated electronic transitions do not correlate very well in terms of energy, usually being under evaluated, the relative ratio of calculated oscillator strength matches very well with the relative ratios measured in experimental intensities between the *meta* and the *para* variants of both complexes and ligands.

In the case of the ligands, both show a very similar absorption spectrum (Figure 3 and Supporting Information, Figure S7), characterized by a broad band around 320 nm and a sharper peak at 260 nm, very near fluorene's maximum intensity peak of 264 nm. Smaller maxima are found near 300 and 290 nm corresponding to other fluorene transitions. The lowest energy transition is seen at 323 nm, very comparable to the nearest fulvene analogue, 9-benzylidenefluorene, with a band at 326 nm, implying very little effect of the heterocyclic ring on the overall electronic delocalization.[29] This transition implies a delocalized $\pi-\pi^*$ transition involving the pyridyl ring. This is confirmed by the TD-DFT calculation, in this case the lower energy transition is at 347 nm (a shift of +26 nm), and in both cases the transitions originate from HOMO and HOMO-1 states, localized on the diphenylfulvene and the pyridine (Supporting Information, Figure S8). For both ligands there is a strong red-shift in the position of the first calculated transition; however, all of the other measured values are in good accordance with the spectra. This is especially true of the relative oscillator strength between ligands; they always follow the same trend as the spectra even if they are far from the experimental absolute values (Table 3). The other major transition at 260 nm only involves fluorene-based molecular orbitals and matches the energy of the calculated transition. It has a 2-fold increase in maximum absorbance vs fluorene molecule (~40000 vs 18000 M^{-1} cm^{-1}).

The low energy absorption and the complete delocalization of the HOMO and LUMO orbitals of both ligands suggest that the fulvene moiety will have an effect on the properties of the associated rhenium chromophores.

In the case of the rhenium complexes (Table 3), the wavelength of the expected mixed singlet metal−ligand-to-ligand charge transfer (MLLCT) transition for pyridine adducts is found around 360 nm with a molar absorptivity of about 5000 M^{-1} cm^{-1}.[12] Note that the MLLCT term is used instead of metal-to-ligand charge transfer (MLCT) term because the implied molecular orbitals of the ground state possess a strong contribution from the carbonyl ligands.[30] Complex **1** only shows a decreasing band at that specific wavelength, but it has twice the molar absorptivity. As can be seen in both Table 3 and Figure 2, the deconvoluted bands of **1** place the first peak maximum at 330 nm, which is the same position as the deconvoluted peak of the ligand. Only the larger width of the band suggests a buried MLLCT band. The MLLCT can be seen more clearly if we compare the spectrum of **1** with a superimposition of the spectra of **3** and ***m*Fpy** (Figure 3). They are almost identical in peak positions, indicating that the tailing in complex **1** above 375 nm is due to the MLLCT of the rhenium bipyridine chromophore.

In contrast, the spectrum of **2** does not superimpose well with the addition of the spectra of the ligand ***p*Fpy** and **3** (Figure 3). There is a new band at 270 nm (43000 M^{-1} cm^{-1}) of comparable intensity with the band at 260 nm (44000 M^{-1} cm^{-1}) and the expected band at 330 nm is shifted to 364 nm

dx.doi.org/10.1021/ic301559s | *Inorg. Chem.* 2012, 51, 12738−12747

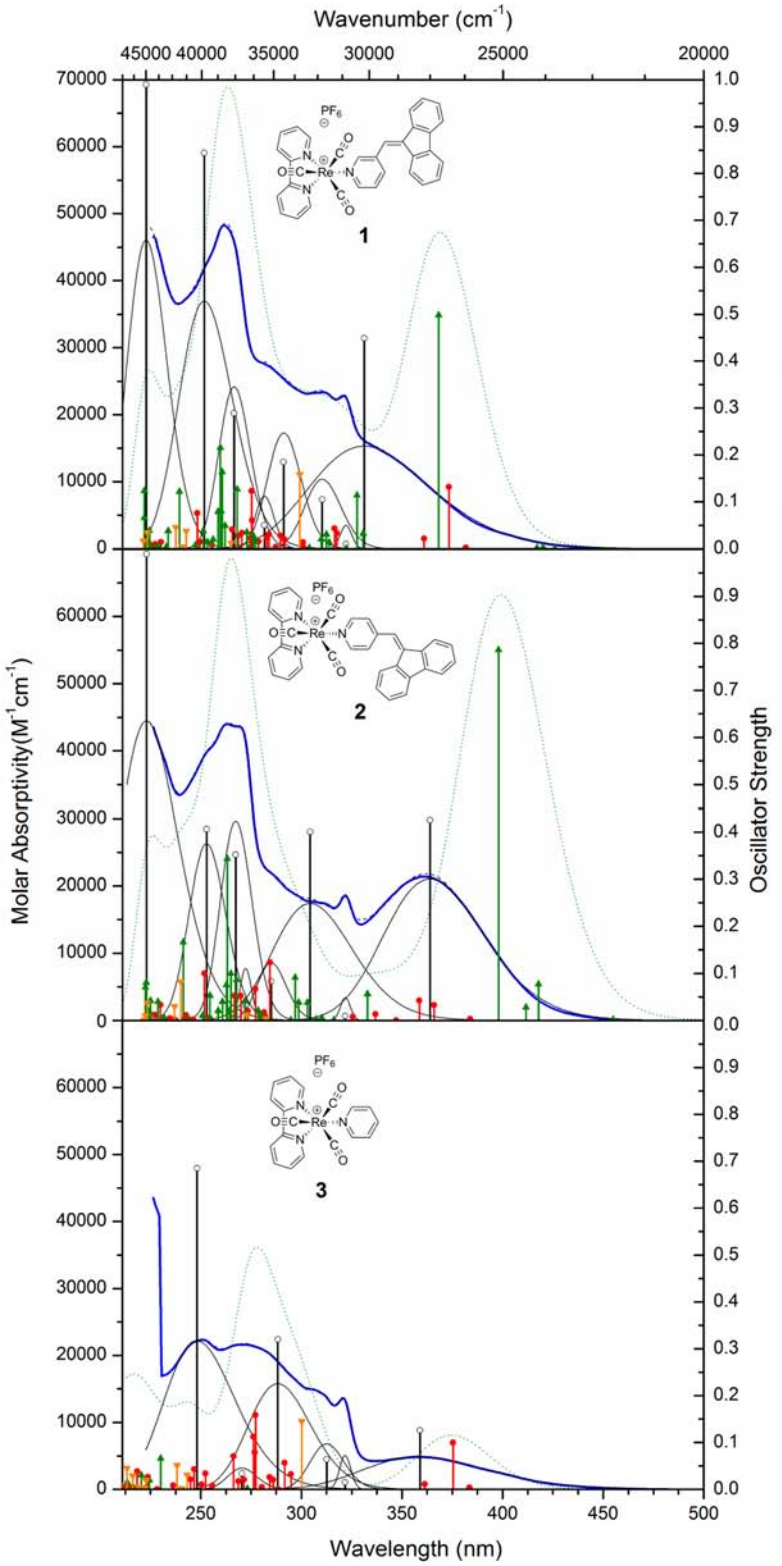

Figure 2. Absorption spectra in dichloromethane of the complexes (in blue; Top: **1**; middle: **2**; bottom: **3**.); Gaussian fits and sum of fits (black; full and dashed); Calculated curves from TD-DFT (dotted green); fitted oscillator strength (black circle); calculated from TD-DFT oscillator strength: Rhenium centered (red disk), Fulvene/pyridine centered (green triangle), bipyridine centered (orange triangle).

(22000 M^{-1} cm^{-1}). This molar absorptivity is four times greater than the pyridyl adduct and suggests a buried MLLCT (~5000 M^{-1} cm^{-1}), hidden beneath a red-shifted ligand-based absorption (~13000 M^{-1} cm^{-1}). A better comparison can be obtained by looking at the oscillator strengths of the implied transitions (Table 3): MLLCT in **3** has a strength of 0.12, the ***p*Fpy**'s $\pi-\pi^*$ transition has 0.25 oscillator strength, for a total of 0.37 versus 0.43 for **2**, a net gain of 0.05 in oscillator strength. This is similar to **1**, for which we have 0.27 for the ligand first transition and 0.45 for the formed complex, again a gain of 0.06 in the oscillator strength.

dx.doi.org/10.1021/ic301559s | *Inorg. Chem.* 2012, 51, 12738−12747

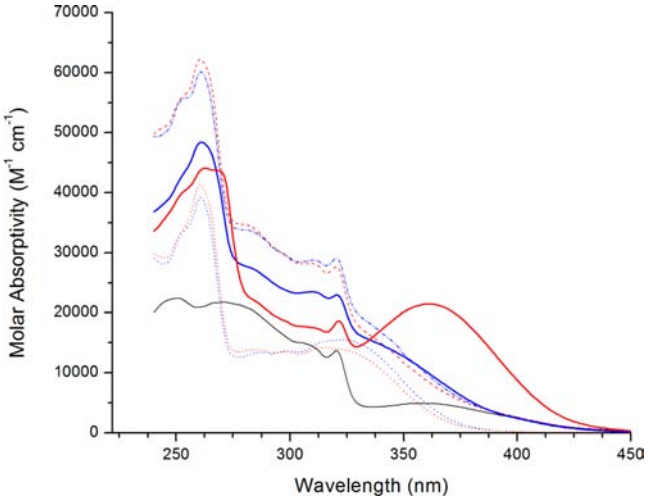

Figure 3. Comparison of the absorption spectra of **1** (blue line), **2** (red line), **3** (black line), ***m*Fpy** (dotted blue line), and ***p*Fpy** (dotted red line) with the additive spectra of **3** and their respective ligand ***m*Fpy** and ***p*Fpy** (dashed blue and red line).

The small gain in both cases can be attributed to an increase in the absorbance cross section of the fulvene brought by the complexation of the rhenium, increasing its polarity.

Another characteristic band of $Re(bpy)(CO)_3L^+$ is the sharp peak at 321 nm; it is present in all of the pyridyl complexes, with a constant oscillator strength, suggesting again that the absorption transitions of the rhenium core are not affected by the fulvene moiety.

All theoretical transitions for the complexes are classified with their implied ground state orbitals as being rhenium-carboxyl, fulvene/pyridine or bipyridine based. This information is visualized in Figure 2 and Supporting Information, Figure S6, and the implied orbitals are visualized in Figure 4. The pyridyl complex (**3**) is the simplest to analyze, looking only at the major calculated oscillator strengths, we can see clearly three features: the MLLCT transition sitting around 375 nm (0.10), a bpy $\pi-\pi^*$ transition at 300 nm (0.14), and other MLLCT transitions at 275 nm (totaling 0.35 oscillator strength). The first two were assigned on the experimental spectra as the transition at 353 nm (0.13) (−22 nm shift) and the transition at 321 nm (0.15) (+21 nm shift). The last transition is not clearly assignable because of the quantity of peaks present at that wavelength, but fits well with the peak at 270 nm (−5 nm) and the measured oscillator strength, 0.68, is a very rough estimate because of the quantity of peaks in the area and its proximity to the upper edge of the spectra.

Complex **1** shows the same transitions as the pyridyl complex: MLLCT at 373 nm (0.13 strength), bipyridine $\pi-\pi^*$ at 299 nm (0.16 strength) and MLLCT transitions centered at 275 nm (0.20 strength). Additional transitions from the fulvene ligand come into play. There is a group of fluorene-based transitions at 260 nm, matching very well with the measured 261 nm transition. Lastly, it has a fulvene $\pi-\pi^*$ transition (HOMO-1 to LUMO+1) at 367 nm (0.50 strength), a +20 nm shift from the calculated ligand absorption. This result does not compare well to the measured maximum of ***m*Fpy** and **1**, 330 and 331 nm, where there is no real shift of the fulvene $\pi-\pi^*$ transition, which suggests that the coordination of the metal has less influence on the delocalization of the fulvene orbital (HOMO-1) contrary to what the calculation indicates. Lastly, it is to note that the lowest energy transition, HOMO to LUMO, has near zero oscillator strength, because of lack of spatial overlap of the ground state and excited

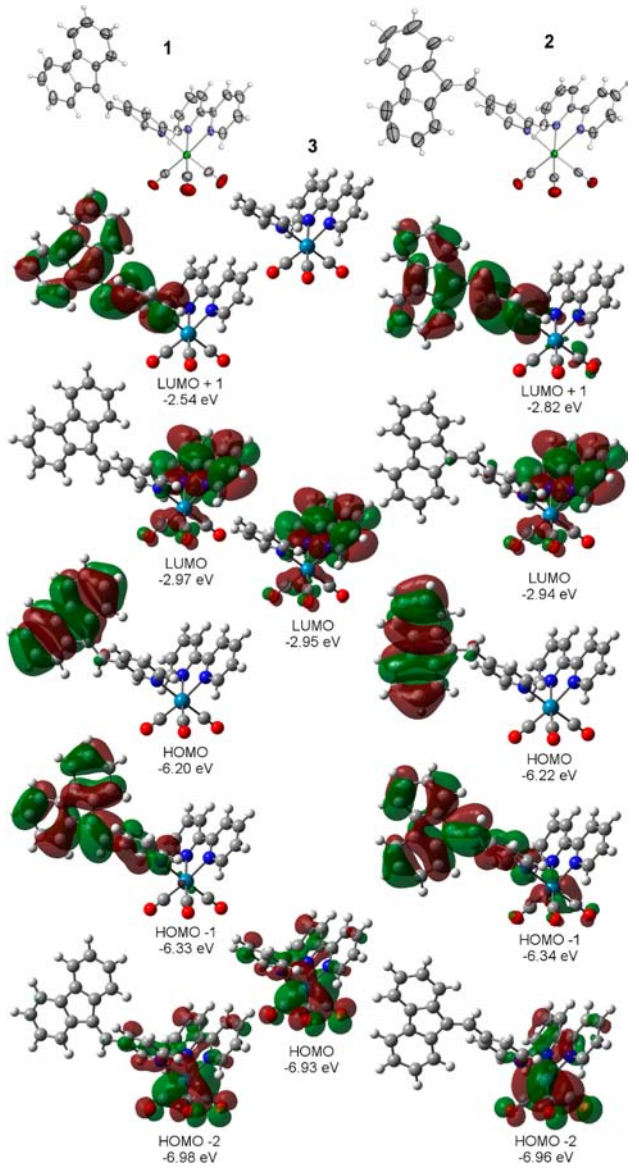

Figure 4. Topmost: ORTEP X-ray crystal structure of **1** (left) and **2** (right) used as starting point for the geometry optimization (50% probability displacement ellipsoids, anion, solvent and other chemically equivalent molecule removed); Top center: optimized structure of **3** starting from crystallographic data.[31] Middle: Frontier molecular orbitals and orbital energies obtained from DFT (rb3lyp/LanL2DZ(f)[Re]6-31G**[C,H,N,O]) CPCM(CH_2Cl_2).

state: the HOMO being localized only on the fluorene moiety is disconnected from the bpy-centered LUMO (Figure 4).

The calculated transitions of **2** differ from the two previous compounds: the lowest permitted transition is the HOMO-1 to LUMO+1 ($\pi-\pi^*$ fulvene centered) at 397 nm (0.87 strength), +50 nm shift from the free ligand. If we compare the measured value, 364 and 327 nm for **1** and ***p*Fpy**, respectively, we have a shift of +34 nm. In this case, the calculation models the extended delocalization in an error of about 20 nm, comparable to the deviation observed for **1**. A closer look of HOMO-1 reveals the origin of the lowering of the transition energy: the HOMO-1 delocalization now extends through the rhenium and the carbonyls; this is not the case for **1**. The extended delocalization also affects the LUMO+1 orbital (LUMO is centered on the bpy in all cases), where in **1** it is centered mainly on bpy and pyridine,

dx.doi.org/10.1021/ic301559s | *Inorg. Chem.* 2012, 51, 12738−12747

and in **2** it is exclusively the delocalized antibonding orbital of ***p*Fpy**. This extended $\pi-\pi^*$ transition leads to a lower energy transition, as observed.

The rest of the calculated transitions of **2** are also affected by this interaction, as indicated by the splitting of the transitions and a greater part of fulvene orbitals being present in the various expected transitions of the Re core. The MLLCT splits to 368 and 358 nm (0.07 total strength); the bpy transition is mixed with a fulvene-based transition at 298 and 302 nm (0.08 total strength). Other noteworthy transitions are the metal-based transition seen at 276 nm (0.07) and finally the fluorene transition, seen at its expected position at 263 nm (0.4 total strength).

Emission and Excited State Theoretical Studies. Neither the ligands nor the complexes emit at room temperature or at 77 K. The closest relative to the pyridylfulvene ligands, 9-benzylidenefluorene, is also reported to have no fluorescence at room temperature or at 77 K.[32] From fluorescence and laser flash photolysis studies, it was reported that the deactivation pathway lies through the triplet state. The transient absorption signal, seen at 450 nm, had a decay of approximately 100 ns. We propose that both ***m*Fpy** and ***p*Fpy** follow this pathway, passing from $^1\pi-\pi^*$ to $^3\pi-\pi^*$ efficiently by intersystem crossing.

As previously mentioned neither complex **1** nor **2** emits, in contrast to the pyridyl analogue **3**, which has a very strong emission at 540 nm (500 nm at 77 K). Solutions of the complexes that stood for several hours did have very weak emission, centered at 545 nm (512 nm at 77 K), but these were proven to be dissociation products attributable to trace $Re(bpy)(CO)_3(solvent)^+$, as seen from the 77 K emission spectra. Note that this dissociation is very small and not perceptible by UV–vis or ^{1}H NMR spectroscopy.

The general absence of a strong emission at low temperature suggests a rapid quenching mechanism of the normally emissive ^{3}MLLCT, suggesting it is no longer the lowest excited energy state. This can be readily rationalized by examining the HOMO and LUMO orbital of the singlet ground state (^{1}GS), the LUMO being a good approximation of the singly occupied molecular orbital (SOMO) in the singlet excited state (^{1}ES) and by identifying the SOMO orbital from the lowest energy triplet excited state (^{3}ES) of the molecule, obtained with a DFT optimization of the triplet "ground state". In the case of **3**, the calculated LUMO orbitals suggest a ^{1}ES centered on the bpy (Figure 4, center). This excited state is very similar to the ^{3}ES, assigned to the ^{3}MLLCT transition state, where the SOMO is also centered on the bpy (Figure 5, center). However, the DFT calculation obtained for **1** and **2** shows a HOMO ^{1}GS centered on the fluorene, not the rhenium core (Figure 4, left and right), while the LUMO, representing the ^{1}ES lies on the expected bipyridine moiety. The Re based orbitals are located at lower levels: HOMO−2, −3, and −5 for both complexes. The SOMO and SOMO−1 of the ^{3}ES of both complexes are not centered on the expected bpy, they are instead on the fulvene and the optimized geometry showed a 90° rotation of the fluorene around the vinyl double bond (Figure 5). This twist in the ^{3}ES is reminiscent of 4-styrylpyridine, bound to a rhenium chromophore, which has been extensively studied by high-level calculations.[4k−m] Fulvene's ability to twist is also known and has been studied in detail as well.[6c−f] The measured triplet energy of unsubstituted pentafulvene is around 2.34 eV (530 nm), and the dibenzofulvene is expected to be lower because of its extended delocalization.[6b] By the difference of total energy calculated from triplet and singlet ground states, the following estimated triplet energy can be made for our complexes:

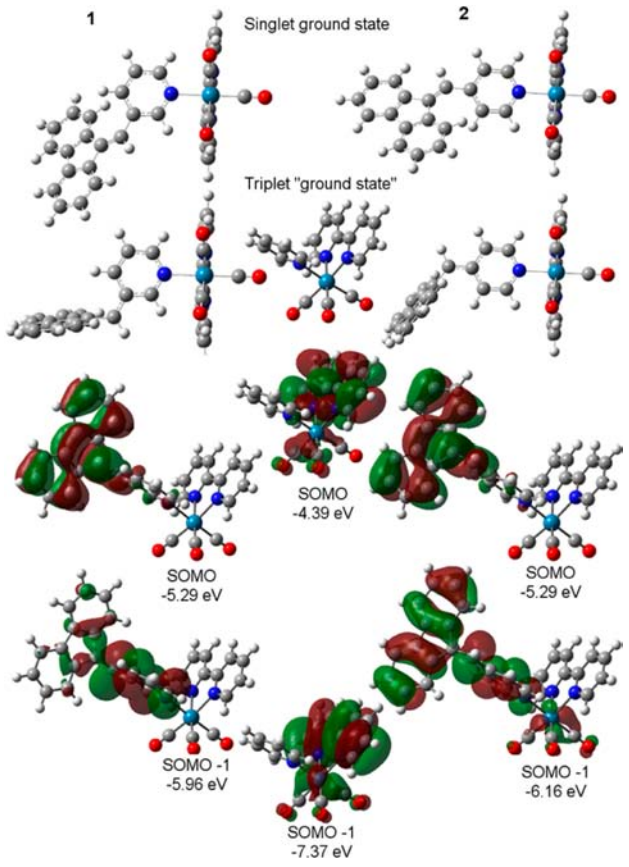

Figure 5. Top: Optimized single vs triplet ground state structure of **1** (left) and **2** (right); Top Center: optimized geometry of **3** triplet ground state; Bottom: SOMO and SOMO−1 molecular orbitals and orbital energies obtained from DFT (ub3lyp/LanL2DZ(f)[Re]6-31G**[C,H,N,O]), CPCM(CH_2Cl_2).

1.52 eV (814 nm) and 1.49 eV (835 nm) for **1** and **2**, while **3** is estimated at 2.76 eV (450 nm) (Supporting Information, Table S1). Although these estimates are approximate (with 50 nm error from the measured emission of **3** at 77 K), they nonetheless suggests an important driving force for the observed quenching of the ^{3}MLLCT emission.

The ^{1}MLLCT state, centered on the bpy ligand, $^1\pi-\pi^*$(fulvene) state, and the whole **Fpy** ligand (including the pyridyl) are very close in energy to each other, the ^{1}MLLCT state being slightly lower energy for **1** and of similar energy for **2**. Furthermore, theses two states are very close spatially, being separated only by the rhenium ion. As such, it is expected that singlet–singlet Dexter energy transfer can occur easily between these states. Both of these excited singlet states can undergo intersystem crossing to their respective triplet state, the MLLCT ISC is very fast, in the order of 200 fs as reported for similar rhenium complexes.[33] A fast triplet–triplet Dexter energy transfer between ^{3}MLLCT and the $^3\pi-\pi^*$-(fulvene) states would follow, as described for 4-styrylpyridine containing rhenium complexes.[33] The non-radiative $^3\pi-\pi^*$-(fulvene) state acts as the sink for the system, since it is of lower energy than the ^{3}MLLCT state. It thus only needs a shorter lifetime than the ^{3}MLLCT to completely quench the emission coming from that state. From literature data, the lifetime of the ^{3}MLLCT of **3**, 669 ns, is longer-lived than the transient lifetime of the closest analogue to our ligand, 9-benzylidenefluorene, at around 100 ns. We propose that the lifetime of the $^3\pi-\pi^*$(fulvene) state of our **Fpy** ligands is

dx.doi.org/10.1021/ic301559s | *Inorg. Chem.* 2012, 51, 12738−12747

similar and leads to the observed quenching.[12,32] Chart 2 illustrate the possible pathways for non-radiative relaxation.

Chart 2. Possible Relaxation Pathways for Complexes 1 and 2

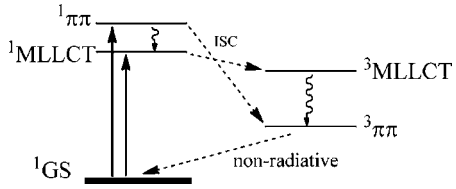

CONCLUSIONS

Incorporating a pyridyl-dibenzofulvene moiety in the coordination sphere of the rhenium(I) complex significantly increases its absorptivity, especially in the case of **2** where the red-shifting of the permitted $^1\pi-\pi^*$ transition of the fulvene ligand is at the same level as the ^{1}MLLCT of the rhenium chromophore. In the case of **1**, the rhenium core has low impact on the fulvene ligand electronic state, as it only increases the absorption of the ligand marginally. From the absence of any fluorescence or phosphorescence of the complex, we can postulate that the fulvene ligand has a non-emissive triplet state of lower energy then the ^{3}MLLCT of the rhenium core, and a fast energy transfer occurs between these two states. This non-emissive triplet state of the fulvene can lead to isomerization. Of course, in this case, no net structural change has occurred, but a small modification on either side of the fluorene would confirm if the implied fulvene triplet non-radiative deactivation pathway occurs through the expected photoisomerization. With the break in symmetry, electronic spectroscopy or NMR can monitor the isomerization. Further studies of this quenching would prove interesting, since the addition of the rhenium complex can lead to an increased isomerization quantum yield to the fulvene class of photoisomers.

ASSOCIATED CONTENT

Supporting Information

X-ray crystallographic data in CIF format, extra figures, and computational data. This material is available free of charge via the Internet at http://pubs.acs.org.

AUTHOR INFORMATION

Corresponding Author

*E-mail: garry.hanan@umontreal.ca. Tel: 1-514-340-5156. Fax: 1-514-343-7586.

Notes

The authors declare no competing financial interest.

ACKNOWLEDGMENTS

We are grateful to the Natural Sciences and Engineering Research Council of Canada, the Ministère de l'Éducation du Québec, and the Université de Montréal for financial support and for the Université de Montréal's Altix super computer supported by le Réseau Québécois de Calculs de Haute Performances (RQCHP) for computer calculations.

REFERENCES

(1) (a) Wrighton, M.; Morse, D. L. *J. Am. Chem. Soc.* **1974**, *96*, 998. (b) Caspar, J. V.; Sullivan, B. P.; Meyer, T. J. *Inorg. Chem.* **1984**, *23*, 2104. (c) Kalyanasundaram, K. *J. Chem. Soc., Faraday Trans. 2* **1986**, *82*, 2401. (d) Lees, A. J. *Chem. Rev.* **1987**, *87*, 711. (e) Sacksteder, L.; Zipp, A. P.; Brown, E. A.; Streich, J.; Demas, J. N.; DeGraff, B. A. *Inorg. Chem.* **1990**, *29*, 4335. (f) Stufkens, D. J.; Vlcek, A., Jr. *Coord. Chem. Rev.* **1998**, *177*, 127. (g) Kirgan, R. A.; Sullivan, B. P.; Rillema, D. P. *Top. Curr. Chem.* **2007**, *281*, 45. (h) Takeda, H.; Koike, K.; Morimoto, T.; Inumaru, H.; Ishitani, O. *Adv. Inorg. Chem.* **2011**, *63*, 137.

(2) (a) Hawecker, J.; Lehn, J. M.; Ziessel, R. *J. Chem. Soc., Chem. Commun.* **1983**, 536. (b) Fihri, A.; Artero, V.; Pereira, A.; Fontecave, M. *Dalton Trans.* **2008**, 5567. (c) Probst, B.; Kolano, C.; Hamm, P.; Alberto, R. *Inorg. Chem.* **2009**, *48*, 1836. (d) Probst, B.; Guttentag, M.; Rodenberg, A.; Hamm, P.; Alberto, R. *Inorg. Chem.* **2011**, *50*, 3404.

(3) (a) Kurz, P.; Probst, B.; Spingler, B.; Alberto, R. *Eur. J. Inorg. Chem.* **2006**, 2966. (b) Takeda, H.; Koike, K.; Inoue, H.; Ishitani, O. *J. Am. Chem. Soc.* **2008**, *130*, 2023. (c) Benson, E. E.; Kubiak, C. P.; Sathrum, A. J.; Smieja, J. M. *Chem. Soc. Rev.* **2009**, *38*, 89. (d) Yui, T.; Tamaki, Y.; Sekizawa, K.; Ishitani, O. *Top. Curr. Chem.* **2011**, *303*, 151. (e) Kumar, B.; Smieja, J. M.; Sasayama, A. F.; Kubiak, C. P. *Chem. Commun.* **2012**, *48*, 272.

(4) (a) Lewis, J. D.; Perutz, R. N.; Moore, J. N. *Chem. Commun.* **2000**, 1865. (b) Sun, S.-S.; Robson, E.; Dunwoody, N.; Silva, A. S.; Lees, A. J.; Brinn, I. M. *Chem. Commun.* **2000**, 201. (c) Yam, V. W.-W.; Zhang, Y. Y. J.; Chu, B. W.-K.; Zhu, N. *Organometallics* **2001**, *20*, 4911. (d) Sun, S.-S.; Lees, A. J. *Organometallics* **2002**, *21*, 39. (e) Dattelbaum, D. M.; Itokazu, M. K.; Iha, N. Y. M.; Meyer, T. J. *J. Phys. Chem. A* **2003**, *107*, 4092. (f) Wenger, O. S.; Henling, L. M.; Day, M. W.; Winkler, J. R.; Gray, H. B. *Inorg. Chem.* **2004**, *43*, 2043. (g) Patrocinio, A. O. T.; Brennaman, M. K.; Meyer, T. J.; Murakami Iha, N. Y. *J. Phys. Chem. A* **2010**, *114*, 12129. (h) Frin, K. P. M.; Murakami Iha, N. Y. *Inorg. Chim. Acta* **2011**, *376*, 531. (i) Lin, J. L.; Chen, C. W.; Sun, S. S.; Lees, A. J. *Chem. Commun.* **2011**, *47*, 6030. (j) Kumar, A.; Sun, S.-S.; Lees, A. J. *Top. Organomet. Chem.* **2010**, *29*, 1. (k) Bossert, J.; Daniel, C. *Chem.—Eur. J.* **2006**, *12*, 4835. (l) Gindensperger, E.; Koppel, H.; Daniel, C. *Chem. Commun.* **2010**, *46*, 8225. (m) Kayanuma, M.; Daniel, C.; Köppel, H.; Gindensperger, E. *Coord. Chem. Rev.* **2011**, *255*, 2693.

(5) (a) O'Donnell, J. L.; Zuo, X.; Goshe, A. J.; Sarkisov, L.; Snurr, R. Q.; Hupp, J. T.; Tiede, D. M. *J. Am. Chem. Soc.* **2007**, *129*, 1578. (b) Cooke, M. W.; Chartrand, D.; Hanan, G. S. *Coord. Chem. Rev.* **2008**, *252*, 903. (c) Casanova, M.; Zangrando, E.; Iengo, E.; Alessio, E.; Indelli, M. T.; Scandola, F.; Orlandi, M. *Inorg. Chem.* **2008**, *47*, 10407. (d) Chartrand, D.; Hanan, G. S. *Chem. Commun.* **2008**, 727. (e) Thanasekaran, P.; Lee, C.-C.; Lu, K.-L. *Acc. Chem. Res.* **2012**, *45*, 1403.

(6) (a) Waldeck, D. H. *Chem. Rev.* **1991**, *91*, 415. (b) Asmis, K. R.; Allan, M.; Schafer, O.; Fuelscher, M. *J. Phys. Chem. A* **1997**, *101*, 2089. (c) Barr, J. W.; Bell, T. W.; Catalano, V. J.; Cline, J. I.; Phillips, D. J.; Procupez, R. *J. Phys. Chem. A* **2005**, *109*, 11650. (d) Alfalah, S.; Belz, S.; Deeb, O.; Leibscher, M.; Manz, J.; Zilberg, S. *J. Chem. Phys.* **2009**, *130*, 124318/1. (e) Ioffe, I.; Dobryakov, A. L.; Granovsky, A. A.; Ernsting, N. P.; Perez, L. J. L. *ChemPhysChem* **2011**, *12*, 1860. (f) Blancafort, L.; Gatti, F.; Meyer, H.-D. *J. Chem. Phys.* **2011**, *135*, 134303/1. (g) Belz, S.; Grohmann, T.; Leibscher, M. *J. Chem. Phys.* **2009**, *131*, 034305/1.

(7) (a) Passalacqua, R.; Loiseau, F.; Campagna, S.; Fang, Y.-Q.; Hanan, G. S. *Angew. Chem., Int. Ed.* **2003**, *42*, 1608. (b) Wang, J.; Hanan, G. S.; Loiseau, F.; Campagna, S. *Chem. Commun.* **2004**, 2068. (c) Wang, J.; Fang, Y.-Q.; Bourget-Merle, L.; Polson, M. I. J.; Hanan, G. S.; Juris, A.; Loiseau, F.; Campagna, S. *Chem.—Eur. J.* **2006**, *12*, 8539. (d) Tyson, D. S.; Luman, C. R.; Zhou, X.; Castellano, F. N. *Inorg. Chem.* **2001**, *40*, 4063. (e) Wang, J.; Fang, Y.-Q.; Hanan, G. S.; Loiseau, F.; Campagna, S. *Inorg. Chem.* **2005**, *44*, 5. (f) Simon, J. A.; Curry, S. L.; Schmehl, R. H.; Schatz, T. R.; Piotrowiak, P.; Jin, X.; Thummel, R. P. *J. Am. Chem. Soc.* **1997**, *119*, 11012. (g) Ford, W. E.; Rodgers, M. A. J. *J. Phys. Chem.* **1992**, *96*, 2917.

(8) (a) Westmoreland, T. D.; Le Bozec, H.; Murray, R. W.; Meyer, T. J. *J. Am. Chem. Soc.* **1983**, *105*, 5952. (b) Westmoreland, T. D.; Schanze, K. S.; Neveux, P. E., Jr.; Danielson, E.; Sullivan, B. P.; Chen, P.; Meyer, T. J. *Inorg. Chem.* **1985**, *24*, 2596. (c) Chen, P.;

Westmoreland, T. D.; Danielson, E.; Schanze, K. S.; Anthon, D.; Neveux, P. E., Jr.; Meyer, T. J. *Inorg. Chem.* **1987**, *26*, 1116.
(9) Connelly, N.; Geiger, W. *Chem. Rev.* **1996**, *96*, 877.
(10) Schmidt, S. P.; Trogler, W. C.; Basolo, F.; Urbancic, M. A.; Shapley, J. R. In *Inorganic Syntheses*; John Wiley & Sons, Inc.: New York, 2007; p 41.
(11) Hevia, E.; Perez, J.; Riera, V.; Miguel, D.; Kassel, S.; Rheingold, A. *Inorg. Chem.* **2002**, *41*, 4673.
(12) Caspar, J. V.; Meyer, T. J. *J. Phys. Chem.* **1983**, *87*, 952.
(13) Casey, C. P.; O'Connor, J. M. *Organometallics* **1985**, *4*, 384.
(14) Plater, M. J.; Kemp, S.; Lattmann, E. *J. Chem. Soc., Perkin Trans. 1* **2000**, 971.
(15) (a) Buu-Hoi, N. P.; Delbarre, F.; Jacqugnon, P.; Brouilhet, H.; Rose, A.; Sabathier, J. F.; Sinh, M. P. *Recl. Trav. Chim. Pays-Bas* **1963**, *82*, 1047. (b) Kolyadina, N. M.; Soldatenkov, A. T.; Gridunova, G. V.; Prostakov, N. S. *Chem. Heterocycl. Compd.* **1999**, *34*, 833.
(16) Ulmschneider, S.; Mueller-Vieira, U.; Klein, C. D.; Antes, I.; Lengauer, T.; Hartmann, R. W. *J. Med. Chem.* **2005**, *48*, 1563.
(17) Frisch, M. J.; Trucks, G. W.; Schlegel, H. B.; Scuseria, G. E.; Robb, M. A.; Cheeseman, J. R.; Montgomery, J., J. A.; Vreven, T.; Kudin, K. N.; Burant, J. C.; Millam, J. M.; Iyengar, S. S.; Tomasi, J.; Barone, V.; Mennucci, B.; Cossi, M.; Scalmani, G.; Rega, N.; Petersson, G. A.; Nakatsuji, H.; Hada, M.; Ehara, M.; Toyota, K.; Fukuda, R.; Hasegawa, J.; Ishida, M.; Nakajima, T.; Honda, Y.; Kitao, O.; Nakai, H.; Klene, M.; Li, X.; Knox, J. E.; Hratchian, H. P.; Cross, J. B.; Bakken, V.; Adamo, C.; Jaramillo, J.; Gomperts, R.; Stratmann, R. E.; Yazyev, O.; Austin, A. J.; Cammi, R.; Pomelli, C.; Ochterski, J. W.; Ayala, P. Y.; Morokuma, K.; Voth, G. A.; Salvador, P.; Dannenberg, J. J.; Zakrzewski, V. G.; Dapprich, S.; Daniels, A. D.; Strain, M. C.; Farkas, O.; Malick, D. K.; Rabuck, A. D.; Raghavachari, K.; Foresman, J. B.; Ortiz, J. V.; Cui, Q.; Baboul, A. G.; Clifford, S.; Cioslowski, J.; Stefanov, B. B.; Liu, G.; Liashenko, A.; Piskorz, P.; Komaromi, I.; Martin, R. L.; Fox, D. J.; Keith, T.; Al-Laham, M. A.; Peng, C. Y.; Nanayakkara, A.; Challacombe, M.; Gill, P. M. W.; Johnson, B.; Chen, W.; Wong, M. W.; Gonzalez, C.; Pople, J. A. *Gaussian 03*, Revision C.02; Gaussian, Inc.: Wallingford, CT, 2004.
(18) (a) Lee, C.; Yang, W.; Parr, R. G. *Phys. Rev. B: Condens. Matter* **1988**, *37*, 785. (b) Becke, A. D. *J. Chem. Phys.* **1993**, *98*, 5648.
(19) (a) Hay, P. J.; Wadt, W. R. *J. Chem. Phys.* **1985**, *82*, 299. (b) Ehlers, A. W.; Boehme, M.; Dapprich, S.; Gobbi, A.; Hoellwarth, A.; Jonas, V.; Koehler, K. F.; Stegmann, R.; Veldkamp, A.; et al. *Chem. Phys. Lett.* **1993**, *208*, 111.
(20) Cossi, M.; Rega, N.; Scalmani, G.; Barone, V. *J. Comput. Chem.* **2003**, *24*, 669.
(21) O'Boyle, N. M.; Tenderholt, A. L.; Langner, K. M. *J. Comput. Chem.* **2008**, *29*, 839.
(22) (a) Sheldrick, G. M. *SADABS*, version 2008/1; Bruker AXS Inc.: Madison, WI, 2008. (b) *SAINT*, version 7.68A; Bruker AXS Inc.: Madison, WI, 2009.
(23) Sheldrick, G. M. *Acta Crystallogr., Sect. A: Found. Crystallogr.* **2008**, *A64*, 112.
(24) (a) Farrugia, L. J. *J. Appl. Crystallogr.* **1997**, *30*, 565. (b) *POV-Ray*, version 3.6; Persistence of Vision Pty. Ltd.: Williamstown, Victoria, Australia, 2004.
(25) Casanova, M.; Zangrando, E.; Munini, F.; Iengo, E.; Alessio, E. *Dalton Trans.* **2006**, 5033.
(26) Kuehn, F. E.; Zuo, J.-L.; Fabrizi de Biani, F.; Santos, A. M.; Zhang, Y.; Zhao, J.; Sandulache, A.; Herdtweck, E. *New J. Chem.* **2004**, *28*, 43.
(27) Bergmann, E. D.; Hoarau, J.; Pacault, A.; Pullman, A.; Pullman, B. *J. Chim. Phys. Phys.-Chim. Biol.* **1952**, *49*, 474.
(28) Baková, R.; Chergui, M.; Daniel, C.; Vlček, A., Jr; Záliš, S. *Coord. Chem. Rev.* **2011**, *255*, 975.
(29) Neuenschwander, M.; Voegeli, R.; Fahrni, H. P.; Lehmann, H.; Ruder, J. P. *Helv. Chim. Acta* **1977**, *60*, 1073.
(30) Massi, M.; Werrett, M. V.; Chartrand, D.; Gale, J. D.; Hanan, G. S.; MacLellan, J. G.; Muzzioli, S.; Raiteri, P.; Skelton, B. W.; Silberstein, M.; Stagni, S. *Inorg. Chem.* **2011**, *50*, 1229.
(31) Oshin, K.; Landis, A. M.; Smucker, B. W.; Eichhorn, D. M.; Rillema, D. P. *Acta Crystallogr., Sect. E* **2004**, *E60*, m1126.
(32) Dufresne, S.; Skalski, T.; Skene, W. G. *Can. J. Chem.* **2011**, *89*, 173.
(33) Vlček, A.; Busby, M. *Coord. Chem. Rev.* **2006**, *250*, 1755.